electronics

MDPI

Article

Structure Design and Reliable Acquisition of Burst Spread Spectrum Signals Without Physical Layer Synchronization Overhead

Shenfu Pan [1], Leyu Yin [1,*], Yunhua Tan [2] and Yan Wang [1]

[1] The 54th Research Institute of China Electronics Technology Group Corporation, Shijiazhuang 050081, China; 15651879079@163.com (S.P.); 287888326@163.com (Y.W.)
[2] School of Electronics, Peking University, Beijing 100871, China; tanggeric@pku.edu.cn
* Correspondence: yinly0531@163.com

Abstract: In order to improve the concealment and security of a point-to-point transparent forwarding satellite communication system, a signal structure based on aperiodic long code spread spectrum is designed in this paper. This structure can achieve reliable signal acquisition without special physical layer synchronization overhead, which can effectively shorten signal transmission time and improve the concealment of communication. In addition, the performance of burst spread spectrum signal acquisition is analyzed in detail by establishing a mathematical model, and the influencing factors and design criteria of the matching filter length for aperiodic long code acquisition are determined. On this basis, a matched filter acquisition method based on high-power clock multiplexing and an adaptive decision threshold design method based on an auxiliary channel are proposed. The above methods effectively reduce hardware complexity and resource consumption caused by long code acquisition, and realize reliable acquisition under the condition of low SNR. The simulation results show that under the condition of Eb/N0 = 3 dB, the transmission efficiency for a 128-symbol burst frame can be increased by 50%, thereby significantly reducing the burst communication time. Furthermore, the acquisition success probability can reach 99.99%.

Keywords: burst spread spectrum; no synchronization overhead; acquisition; adaptive threshold

check for updates

Citation: Pan, S.; Yin, L.; Tan, Y.; Wang, Y. Structure Design and Reliable Acquisition of Burst Spread Spectrum Signals Without Physical Layer Synchronization Overhead. *Electronics* **2024**, *13*, 4586. https://doi.org/10.3390/electronics13234586

Academic Editor: Dimitra I. Kaklamani

Received: 9 October 2024
Revised: 9 November 2024
Accepted: 15 November 2024
Published: 21 November 2024

Copyright: © 2024 by the authors. Licensee MDPI, Basel, Switzerland. This article is an open access article distributed under the terms and conditions of the Creative Commons Attribution (CC BY) license (https://creativecommons.org/licenses/by/4.0/).

1. Introduction

Satellite communication has many advantages. It has a large communication coverage area, long communication distance, and the cost of building a station is almost independent of the communication distance. Besides this, it also has flexible networking, large communication capacity, good communication quality, strong reliability, etc. This paper focuses on the satellite communication system of UAVs and submarines, which uses a geosynchronous high orbit (GEO) satellite. It is well known that three satellites can achieve global coverage, which means only one satellite can achieve long-distance communication within 2000 km. The scenario in this paper adopts transparent forwarding and uses a custom private satellite communication protocol. We take the satellite-drone communication model as an example, as shown in Figure 1 below. The space and weight of platforms such as drones are severely limited, so a single input and a single output are usually used. Besides this, the caliber of the airborne antenna is usually less than 0.3 m. The signal frequency is in the ka/ku band. The SNR received by the airborne terminal is about 5–8 dB. Due to the influence of rain fade in the channel, the attenuation of the SNR should be considered. Therefore, in practical scenarios, reliable communication in the SNR of 3 dB should be satisfied at least.

For submarine and unmanned aerial vehicle satellite communication systems, as well as submarines and unmanned aerial vehicles used as stealth combat platforms, the communication system is required to have strong concealment, anti-interference and reliability. This is especially true for satellite communication based on transparent forwarding, because

the channel is open, the signal in the communication process is vulnerable to eavesdropping and interception, and there are serious security threats such as the positioning of the combat platform and the acquisition of business information by the other party. The longer the exposure time, the higher the security risk. Burst spread spectrum combines the advantages of the low spectral density of spread spectrum signals and the short duration of burst communication, which is an effective anti-interception communication technique. Therefore, most UAV and submarine satellite communication systems adopt the burst spread spectrum communication mode at present.

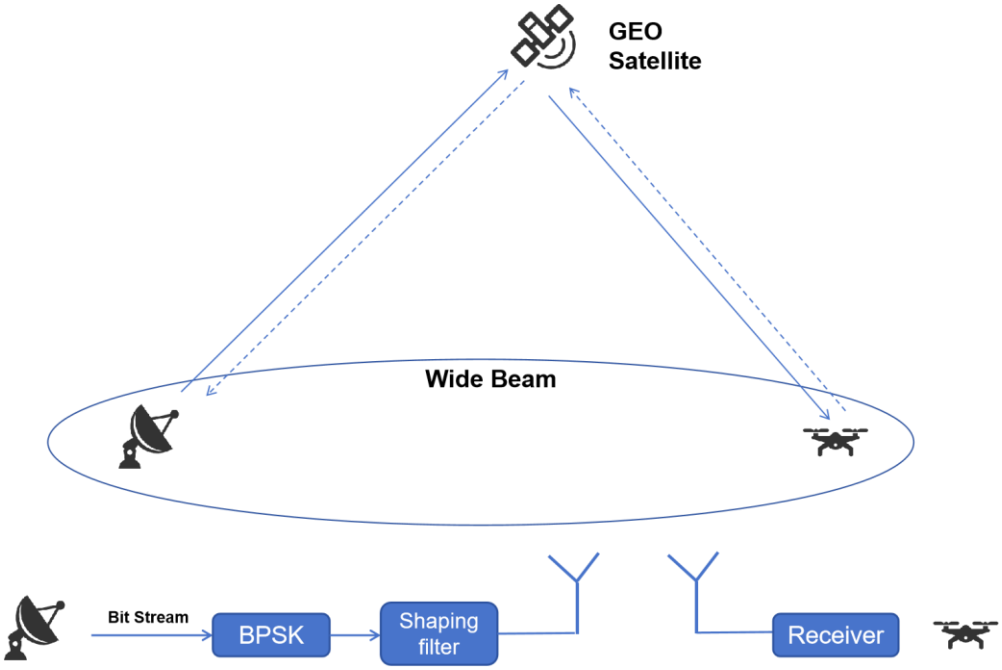


Figure 1. Satellite communication scenario.

Due to the randomness and temporality of burst spread spectrum communication, synchronization overhead is usually added to the physical layer to realize synchronization. The frame structure diagram of the physical layer of a typical burst spread spectrum signal is shown in Figure 2. A burst physical frame is usually composed of synchronous overhead and effective data, in which the effective data refer to modulation symbols after channel coding and symbol mapping. Synchronous overhead usually adopts a specific modulation symbol for a spread spectrum, which is generally composed of three parts, as follows: synchronization field 1 is used for spread spectrum code synchronization; synchronization field 2 is used for carrier frequency offset estimation and carrier initial phase estimation; synchronization field 3 is used to locate the start time of valid data. L is the total length of overhead 1, 2 and 3. $L1$ must be at least 64 bytes, and $L = L1 + L2 + L3$ must be at least 128 bytes [1,2].

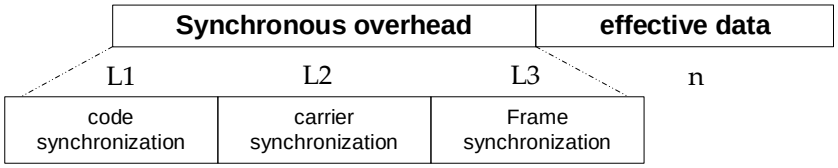


Figure 2. Physical layer frame structure of a typical burst spread spectrum signal.

The burst spread spectrum based on synchronous overhead usually adopts periodic code, and the burst spread spectrum signal is a fixed-length frame signal structure. The baseband signal processing process at the sending end (before he shaping filter) is shown

in Figure 3. Here, N is the spread spectrum multiple, n is the length of effective data, and Rc is the code rate.

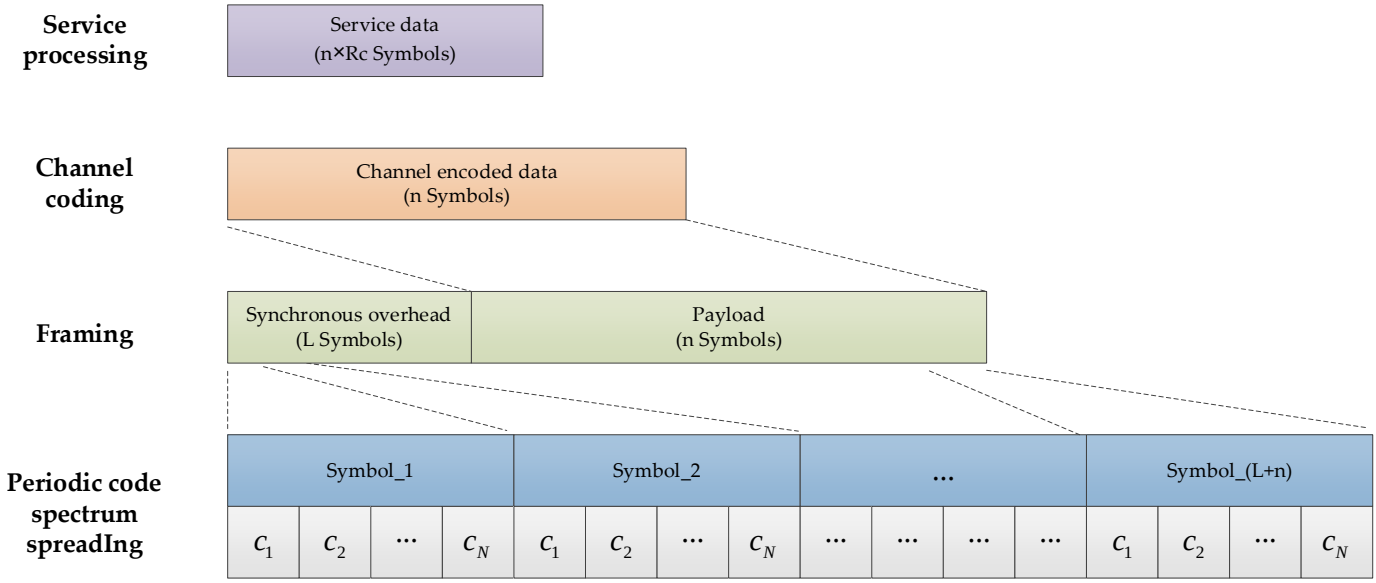


Figure 3. The processing flow of burst spread spectrum signal based on synchronous overhead.

The method based on synchronization overhead can make the process of signal synchronization simpler, but it will reduce the efficiency of information transmission. In particular, submarine and UAV satellite communication systems have the special conditions of low SNR and large carrier frequency offset application [3,4]. In order to achieve the correct synchronization of the carrier, usually a long synchronization header is needed, that is, long auxiliary data for capturing and synchronizing the carrier must be included in a burst frame. This will increase the synchronization overhead of the burst communication system, affect the communication efficiency, increase the signal space exposure time, and increase the probability of being intercepted. Removing the overhead of the synchronous head can greatly improve the transmission efficiency, shorten the airborne exposure time of the signal, and further improve the anti-interception performance of the communication.

At present, most burst spread spectrum systems realize synchronization based on synchronization overhead. Paper [5–11] uses the synchronization overhead of the leading code, frame header, special synchronization sequence and pilot frequency to realize system synchronization. However, no synchronization overhead is only realized in multiple-input multiple-output (MIMO) systems, which can achieve no synchronization overhead through the correlation of multiple signals [12]. The removal of the synchronization cost in single-input single-output spread spectrum systems only focuses on the carrier synchronization part, such as by using non-data-assisted methods [13], or it just focuses on removing frame synchronization overhead, as in paper [14]. The proposed method in this paper can improve the frame transmission efficiency by removing the synchronization overhead of the physical layer, and better complement the gaps in related fields.

The length and complexity of synchronization overhead are related to the acquisition mode, frequency offset, dynamics, SNR and so on. Burst spread spectrum communication has the characteristics of low power spectrum density, short burst time and random transmission time. Therefore, the system response time is required to be short enough, that is, the receiver should be able to quickly acquire the signal, demodulate the original signal, and wait for the arrival of the next signal. This puts forward a high requirement for the real-time operation and probability of spread spectrum code acquisition.

To remove the physical layer synchronization overhead and ensure synchronization, an aperiodic long code spread spectrum is used. However, the acquisition of aperiodic long

codes has the problem of high hardware resource usage, so it is necessary to ensure the capture success rate and reduce the hardware resource usage.

Typical acquisition methods include sliding correlation, a matching filter, FFT, PMF-FFT, and so on. However, the sliding correlation method is slow and the search time is long, which can meet the requirement of fast acquisition set in this paper. The hardware complexity of the matching filter method is high, and the time domain correlation value is large, which is proportional to the square of the code period length, so it is not suitable for the long code acquisition in this paper. The FFT algorithm mainly deals with the acquisition of spread spectrum signals under the condition of high dynamic and high SNR [15], and is not applicable to the situation of low SNR in this paper. The PMF-FFT method can shorten the length of a single matching filter by increasing the number of matching filters, but it cannot effectively reduce the hardware resource consumption [16,17].

Aiming at long code acquisition, paper [18–20] studies the indirect acquisition method of short-code-assisted long code acquisition. However, when indirect acquisition is adopted, the short code with poor anti-interference ability is easily disturbed. Long codes cannot be captured once interfered with, which means they cannot meet the anti-interference requirements of the transparent forwarding satellite communication system in this paper. In addition, refs. [21–24] adopt the direct acquisition method of XFAST and use overlapping codes to perform correlation operations on the received signals. However, the folding process of local pseudo-codes will increase the mutual interference between pseudo-codes and reduce the sensitivity. Therefore, this method is more suitable for acquisition under the condition of high SNR, but not suitable for the condition of low SNR in this paper.

None of the existing acquisition methods can meet the requirements of acquisition success rate and hardware resource occupation at low SNR. Therefore, a matching filter acquisition method based on high-power clock multiplexing is proposed, and the adaptive decision threshold design method based on auxiliary channels is used to achieve the reliable acquisition of a spread spectrum code under the condition of low SNR.

Based on the above ideas, the main contributions of this paper are as follows:

- The synchronization head overhead is removed to improve transmission efficiency—a burst spread spectrum signal design method using an aperiodic long code spread spectrum is proposed, and a signal model without physical layer synchronization overhead is constructed;
- Reliable acquisition is ensured while eliminating synchronization overhead—the acquisition strategy of the aperiodic long code spread spectrum signal is given, and the factors affecting the acquisition performance are analyzed in detail;
- The hardware resource complexity problem caused by aperiodic long code acquisition is effectively solved—the matching filter length design method is analyzed, and a matching filter implementation method based on high-power clock multiplexing is proposed. This method can meet the requirements of resource-limited engineering applications and high security, and has wide application value;
- The reliable acquisition of spread spectrum code under the condition of low SNR is realized—an adaptive decision threshold design method based on auxiliary channels is proposed.

The rest of this paper is organized as follows. Section 2 introduces the design of the structure of a burst spread spectrum signal based on an aperiodic long code. In Section 3, the acquisition performance is analyzed, and the acquisition method of the aperiodic length code without physical layer synchronization overhead is designed. In Section 4, the design and implementation of matching filter length based on high-power clock multiplexing are introduced. In Section 5, an adaptive decision threshold design method based on auxiliary channels is presented. In Section 6, simulation and experimental tests are carried out, and the results are given and discussed. A summarization of this paper is given in Section 7.

2. Burst Spread Spectrum Signal Design Based on Aperiodic Long Code

In order to improve the efficiency of frame transmission, this paper presents a signal design method to remove the synchronous overhead. To remove the synchronization overhead, the signal structure needs to be redesigned. The burst spread spectrum signal without physical layer synchronization overhead adopts an aperiodic long code spread spectrum. The baseband processing process at the signal sender (before shaping filter) is shown in Figure 4.

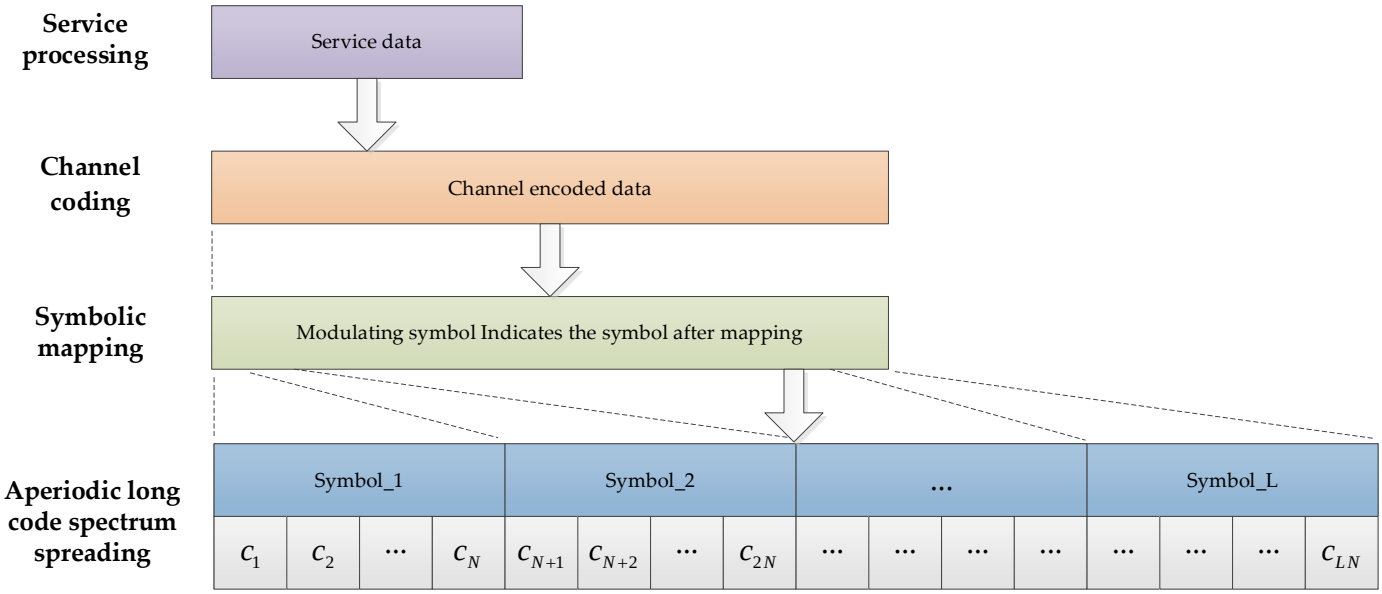


Figure 4. Processing flow of aperiodic long code signal sender without synchronization overhead.

Compared with the burst spread spectrum signal based on synchronous head, there are two main differences. First, there is no special synchronous head. Second, the spread spectrum code adopts an aperiodic length code, which does not repeat in a burst frame. Therefore, as long as the receiver realizes the synchronization of the spread spectrum code and locates the spread spectrum code, the beginning time of the burst signal and the position of the signal in the burst frame are determined. This enables bit synchronization and frame synchronization, and restores the signal structure.

The receiver processing block diagram of the aperiodic long code spread spectrum burst signal without physical layer synchronization overhead is shown in Figure 5. The specific work flow is as follows:

1. Cache the sampled data;
2. Spread spectrum code acquisition—Configure the matching filter parameters to start the spread spectrum code acquisition. The beginning time of the burst signal can be located after the spread spectrum code is captured;
3. Spread spectrum code tracking—After the spread spectrum code synchronization, the data of certain symbol length are taken from the cache for processing to complete the spread spectrum code tracking;
4. Carrier frequency offset correction—The best sampling point data corresponding to a certain symbol length are taken from the cache, and the local spread spectrum code is de-expanded. After the de-expanding, the carrier frequency offset is estimated based on the algorithm assisted by no data, and the estimated results are used to correct the frequency offset of the data in the cache;
5. Carrier phase recovery—After carrier frequency offset correction, the data are read from the cache for frequency conversion, de-expansion and carrier recovery. Because there is no data assistance, the phase ambiguity problem exists in the data after carrier recovery;

6. Extract valid data for channel decoding—Phase ambiguity needs to be identified and corrected during decoding.

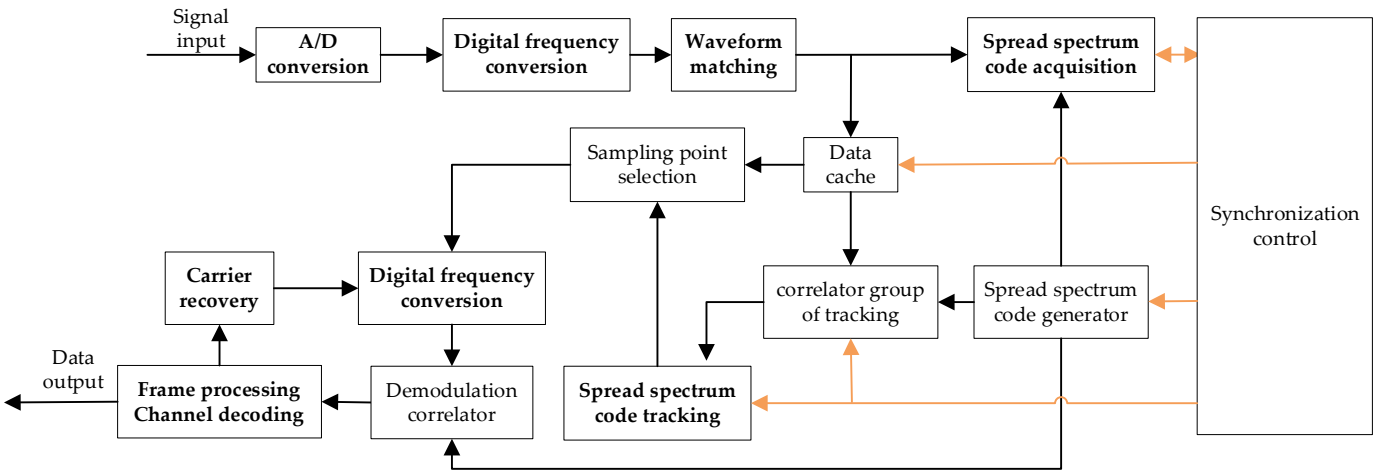


Figure 5. Block diagram of the receiver of burst spread spectrum signal.

The fast and reliable acquisition of an aperiodic long spread spectrum code is the key and most difficult point of receiving and processing burst spread spectrum signals without synchronization overhead of the physical layer. According to the application background of burst spread spectrum acquisition, the acquisition method based on matching filter is adopted. Compared with the burst spread spectrum receiving based on a synchronous head, a higher-order matched filter is needed and the hardware implementation complexity is higher.

The basic principle of using matching filter to achieve spread spectrum code acquisition is as follows. The correlation between the input signal and the local spread spectrum code is carried out in a modulation symbol period, and then the test statistics are obtained by modularization and multiple incoherent accumulations. Then, the test statistics and the threshold are judged to determine whether the input signal and the local spread spectrum code are synchronized, and the acquisition performance is determined by the incoherent accumulation and the decision threshold. Due to the short duration of the burst spread spectrum signal, it is necessary to complete the acquisition quickly and ensure the correctness of the acquisition. Therefore, an incoherent accumulation length and synchronous decision threshold should be reasonably designed for the given SNR constraints and acquisition success probability requirements.

3. Strategy and Performance Analysis of Spread Spectrum Code Acquisition

There is delay and rain attenuation in signal propagation, and satellite communication is exposed to various electromagnetic interferences in space. The satellite channel model can be designed as an ideal Gaussian channel; the SNR reflects the influence of rain decline, the anti-interference ability is enhanced by spread spectrum technology, and the signal synchronization is carried out by acquisition technology.

3.1. Signal Model

The spread spectrum signal waveform can be expressed as $s(t)$, and the chip period is T_c. The receiving end uses the root raised cosine filter to match the $s(t)$ signal, after which the channel response has the raised cosine characteristic [25]. The signal after passing through the matched filter can be expressed as $r(t)$, assuming that the local spread spectrum code is not strictly aligned with the received signal. Then, the normalized spread spectrum code synchronization error is τT_c, where τ is the normalized signal transmission delay. $r(t)$

is sampled at the chip rate at time $t = kT_c$. Considering the complex baseband model under an ideal Gaussian channel, the sampled baseband signal can be expressed as

$$r(k) = As(k)e^{j(2\pi fkT_c+\varphi)} + n(k) \tag{1}$$

where A is the signal amplitude, f is the carrier frequency and φ is the carrier phase after matched filtering. $n(k)$ is the noise after sampling, where $n \sim N(0, \sigma_n^2)$. For detailed expressions, please refer to Appendix A.

3.2. Aperiodic Long Code Acquisition Process

The block diagram of burst spread spectrum code acquisition based on a matched filter is shown in Figure 6.

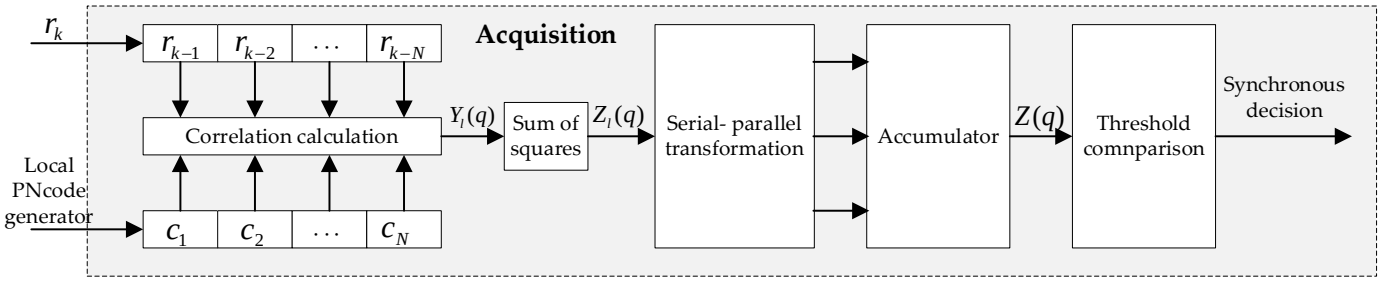


Figure 6. Block diagram of spread spectrum code acquisition based on matched filter.

Assuming that the spread spectrum multiple is N, the following strategies are generally adopted for synchronous acquisition in engineering:

The first step—The local spread spectrum code sequence is correlated with the received signal of different delays, and the sampling of the 2× bit rate clock is performed. There can be $2N$ correlation values in 1 symbol period. Since the spread spectrum code is an aperiodic long code, there are $2NL$ possible correlation values. The expression after correlation is

$$\begin{aligned} Y_l(q) &= \frac{1}{N}\sum_{k=lN}^{(l+1)N-1} c^*(k)r(k-q) \approx Ad_l h(-\tau T_c)\frac{\sin(\pi fT)}{\pi fT}e^{j\varphi_l} + \frac{1}{N}\sum_{k=lN}^{(l+1)N-1} c^*(k)n(k) + n_{2,l}(q) \\ &= Be^{j\varphi_l} + n_{1,l}(q) + n_{2,l}(q) \end{aligned} \tag{2}$$

where $B = Ah(-\tau T_c)\sin c(fT)$. $n_{1,l} \sim N(0, \sigma_n^2/N)$, where $n_{2,l}$ is the noise caused by inter-code crosstalk, which can be ignored. The local spread spectrum code is $c(k)$. q is the number of shift chips, $q = lN, lN + 1/2, \ldots, (l+1)N - 1$. $h(t)$ is the raised cosine function, and $h(-\tau T_c)$ is the amplitude change caused by the code synchronization error. $\sin c(fT)$ is the amplitude change caused by frequency offset. φ_l is code phase. For the relevant calculations, please refer to Appendix B.

Binary hypothesis testing is adopted, where

$$\begin{cases} Y_l(q) = n_{1,l}(q), & H_0 \\ Y_l(q) = Be^{j\varphi_l} + n_{1,l}(q), & H_1 \end{cases} \tag{3}$$

Here, H_0 is set under the condition that the sender does not send a spread spectrum signal or the local code is not aligned with the received signal, and H_1 is set under the condition of the local code being basically aligned with the received signal.

Y_l is a complex signal, where the signal in I channel is Y_I and thesignal in Q channel is Y_Q, and $Y_l = Y_I + jY_Q$. The conjugate multiplication of Y_l yields

$$Z_l(q) = Y_l(q)Y_l^*(q) = \sum Y_I^2(q) + Y_Q^2(q) \tag{4}$$

In the second step, the correlation values, Z_l, obtained in the first step are incoherently accumulated L times, and $2q$ test statistics are obtained,

$$Z(q) = \sum_{l=0}^{L-1} Z_l(q) = \sum_{l=0}^{L-1} Y_I^2(q) + Y_Q^2(q) \tag{5}$$

In the third step, the test statistic $Z(q)$ obtained in the second step is compared with the threshold V_{th}. If the value is greater than the threshold, it is considered as synchronization. If the threshold is not exceeded, the next statistics and judgment are carried out. It is hoped that only 1 of the $2LN$ possible correlation values that are fully synchronized will exceed the threshold.

Let P_n present the noise power σ_n^2/N, and so the symbol signal-to-noise ratio is $\mu = B^2/P_n$. p_0 is the probability density function under the condition of H_0 and p_1 is the probability density function under the condition of H_1. By integrating p_0 and p_1, the unit false alarm probability P_f and unit detection probability P_d of each decision can be obtained. Let the normalized threshold be $\lambda = V_{th}/\sigma_0^2$, according to [5,26]

$$P_f = \int_{V_{th}}^{\infty} p_0(Z)dZ = \int_{\lambda}^{\infty} p_0(z)dz = \int_{\lambda}^{\infty} \frac{x^{L-1}e^{-z}}{(L-1)!}dz = e^{-\lambda}\sum_{k=0}^{L-1}\frac{\lambda^k}{k!} \tag{6}$$

$$P_d = \int_{V_{th}}^{\infty} p_1(Z)dZ = \int_{\lambda}^{\infty} \left(\frac{x}{L\mu}\right)^{(L-1)/2} e^{-(x+L\mu)}\Phi_{L-1}(2\sqrt{L\mu x})dx = Q_L(\sqrt{2L\mu}, \sqrt{2\lambda}) \tag{7}$$

where $Q_L(a,b)$ is an L-order Marcum Q function, which can be solved by calling function $marcumq(a,b,L)$ in matlab. The specific form of this function is [27]

$$Q_L(a,b) = a^{-(L-1)}\int_b^{\infty} x^L e^{-\frac{x^2+a^2}{2}}\Phi_{L-1}(ax)dx \tag{8}$$

The synchronous acquisition of spread spectrum signals based on the above strategies has the following characteristics: a synchronous decision is made for every L symbols, and $2NL$ decisions can traverse all possible spread spectrum code phases. The probability of false acquisition can be reduced under the condition of low SNR.

3.3. Acquisition Success Probability and Incoherent Accumulation Length Analysis

The system false alarm probability is the same as the unit false alarm probability, that is,

$$P_F = P_f \tag{9}$$

As can be seen from Figure 7, if a false alarm occurs in the frame burst period before the successfully captured decision position, the receiver will directly transfer to the tracking state and cancel the acquisition. This will miss the successful acquisition decision position of the burst signal, resulting in a missed signal. If the number of decisions in a period is $M = 2NL$, there will be $M-1$ false alarms of the decision position in the previous frame period of the signal, which may lead to missing alarms. The probability of no missing alarms due to false alarms in the previous frame period is $(1-P_f)^{M-1}$. Then, the system missing probability, that is, the acquisition failure probability, is the missing probability of the correct decision position plus the failure probability caused by false alarms,

$$P_M = (1-P_f)^{M-1}P_m + 1 - (1-P_f)^{M-1} \tag{10}$$

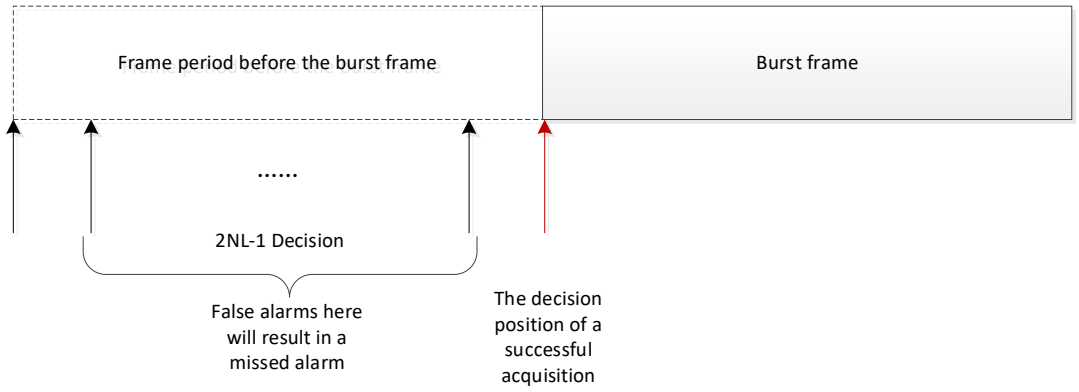


Figure 7. Signal acquisition decision diagram.

Therefore, the acquisition success probability is the system detection probability, which is $M-1$ (no false alarm) and 1 (no missing alarm), and its calculation formula is as follows:

$$\begin{aligned} P_{acq} &= P_D = 1 - P_M = (1 - P_f)^{M-1} P_d \\ &= (1 - e^{-\lambda} \sum_{k=0}^{L-1} \frac{\lambda^k}{k!})^{2NL-1} \quad Q_L(\sqrt{2L\mu}, \sqrt{2\lambda}) \end{aligned} \tag{11}$$

In addition, it can be seen from Equation (11) that the acquisition success probability is jointly determined by the incoherent accumulation length L and the normalized decision threshold λ. The larger the number of incoherent accumulations, the higher the maximum value of P_{acq}, but an increase in L will increase the hardware implementation complexity. Based on the goal of improving the success probability of the acquisition of burst spread spectrum signal, the length L determination method is presented in Section 4.1; a matched filter acquisition implementation method based on high-power clock multiplexing is proposed in Section 4.2 to effectively reduce hardware complexity and resource consumption; and an adaptive decision threshold design method based on the auxiliary channel is proposed in Section 5. Based on the above designs, the success probability of burst spread spectrum acquisition can be optimized.

4. Design and Implementation of Matched Filter Based on High-Power Clock Multiplexing

4.1. Matched Filter Length Design

According to Formula (11), when the length of incoherent accumulations L is fixed, the values of P_{acq} under different normalization thresholds are different, and P_{acq} can reach the maximum at a certain threshold. The maximum value of P_{acq} is different under different incoherent accumulation lengths, and is denoted as $P_{max}(L)$. Increasing the length of incoherent accumulations can improve the success probability of acquisition at suitable thresholds. As can be seen from Figure 8, the larger the length of incoherent accumulations, the larger the $P_{max}(L)$ value, and it gradually tends to 1. According to the requirement of acquisition success probability, when the maximum acquisition success probability under a certain incoherent accumulation length is large enough, the appropriate length of incoherent accumulation can be obtained. A detailed simulation is shown in Section 5.1.

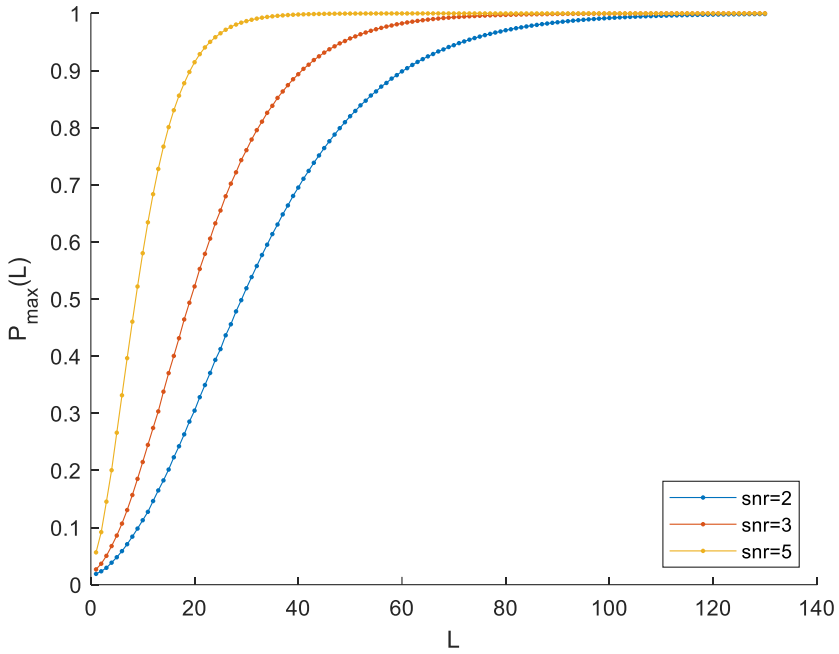


Figure 8. The relationship between the maximum value of P_{acq} and L.

4.2. Implementation of Matched Filter Based on High-Power Clock Multiplexing

Because the increase in length will increase the complexity of hardware implementation, this paper presents a solution of high-power clock multiplexing, which can effectively reduce the resource consumption. Taking 8× clock multiplexing as an example, the structural difference between multiplexing and non-multiplexing is shown in Figure 9.

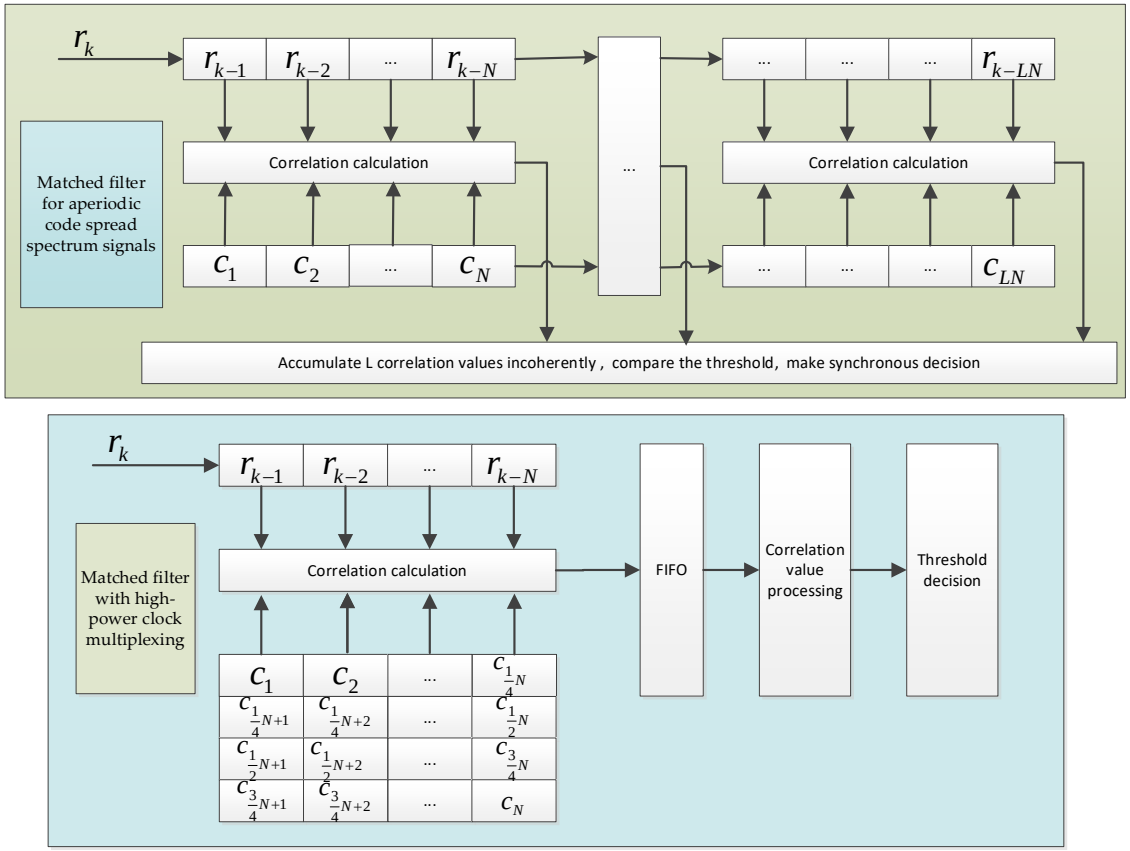


Figure 9. Comparison of non-multiplexed and multiplexed long code matched filters.

We assume that the spread spectrum ratio is N, the number of incoherent accumulations is L, and the system is driven by an $8\times$ code clock (denoted as *sclk*). The minimum code phase step during code acquisition is half the chip width, corresponding to the sampling of the $2\times$ code clock, that is, two sample points per chip. Since the system is driven by $8\times$ code clock (denoted as *sclk*), the duration of each sample point is four *sclk* cycles. Therefore, the length of the shift register of the matched filter input data is designed to be $N/4$. The input signal $r(k)$ is shifted once every four *sclk* cycles, and the register enters a sample point. The length of a symbol after the spread spectrum is N chips, with $2N$ sample points. Therefore, stepping through $2N$ times yields the complete signal after spreading for one symbol.

Since X_l is only updated every four *sclk* cycles, the data in the register can be completely updated every $2N$*sclk* cycles. When the correlation operation is performed, one sample point is taken for each code slice. Using *sclk* drive, four partially relevant values can be obtained during this period,

$$Y_{I,l}(q) = X_l(q)C_I = \sum_{k=IlN/4}^{I(l+1)N/4-1} r(k-q){c_I}^*(k),\ I = 0,1,2,3 \tag{12}$$

where $q = IlN/4, IlN/4 + \frac{1}{2}, \ldots, I(l+1)N/4 - 1$.

After the data in the register are fully updated four times, that is, after $8N$ *sclk* cycles, the fully correlated value of a symbol can be obtained, which can be expressed as

$$Y_l(q) = \sum_{k=lN}^{(l+1)N-1} r(k-q)c^*(k),\ \ where\ q = lN, lN + \frac{1}{2}, \ldots, (l+1)N - 1 \tag{13}$$

In order to save storage resources, FIFO with a depth of $2N$ is designed, and *sclk* is used as the working clock. If the partial correlation value $Y_{I,l}(IlN/4)$ is directly taken as the current input of the FIFO, then the current output of the FIFO is $Y_{I-1,l}((I-1)lN/4)$. Assuming that the input of FIFO is a and the output is b, in order to obtain the fully correlated value of (13), the input design of FIFO is as follows:

$$a = \begin{cases} Y_{I,l}(q) + b, & I \neq 3 \\ 0, & I = 3 \end{cases} \tag{14}$$

Thus, every eight *sclk* cycles (corresponding to one sampling cycle), we can obtain a fully correlated value corresponding to a certain code phase,

$$Y_l(q) = Y_{I,l}(q) + b\,|_{I=3} \tag{15}$$

According to Formula (5), in order to improve the reliability of the synchronous decision, the correlation values of L symbols are incoherently accumulated before the decision. An FIFO with a depth of $2N$ is designed and driven by the sampling clock (2x code clock). If $Z_l(lN)$ is directly taken as the current input to the FIFO, then the current output of the FIFO is $Z_{l-1}((l-1)N)$. Assuming that the input of FIFO is a and the output is b, in order to obtain the decision statistics after cumulation, the input design of FIFO is as follows:

$$a = \begin{cases} Z_l(q) + b, & count < 2N(L-1) \\ 0, & count \geq 2N(L-1) \end{cases} \tag{16}$$

In this way, the $2N$ cumulative decision statistics corresponding to each code phase are obtained in each L symbol period,

$$Z(q) = Z_l(q) + b\,\Big|_{count \geq 2N(L-1)} \tag{17}$$

The result of (17) can be compared with the set threshold to make a synchronous decision. Therefore, in the following section, we design the input threshold.

5. Adaptive Decision Threshold Design Method Based on Auxiliary Channel

In the actual burst spread spectrum communication system, the noise intensity of the channel is constantly changing with time. Therefore, in signal detection, if the fixed threshold is used, it will be difficult to detect the signal correctly and accurately. Therefore, it is necessary to adaptively change the decision threshold according to the strength of the current background noise to maintain a high detection probability [28,29]. At this time, the PN code acquisition of the wireless mobile communication system can be completed only by real-time estimation of the decision threshold according to the statistical characteristics of the test statistics Z [30,31]. Based on the statistical characteristics Z of the test statistic, and the relationship between unit false probability, unit detection probability, acquisition success probability and decision threshold in (6), (7) and (11), an adaptive design method of a decision threshold based on the auxiliary channel is proposed.

The block diagram of the acquisition algorithm based on adaptive threshold decisions is shown in Figure 10. The acquisition threshold Vth is related to the normalized threshold λ and noise power P_n.

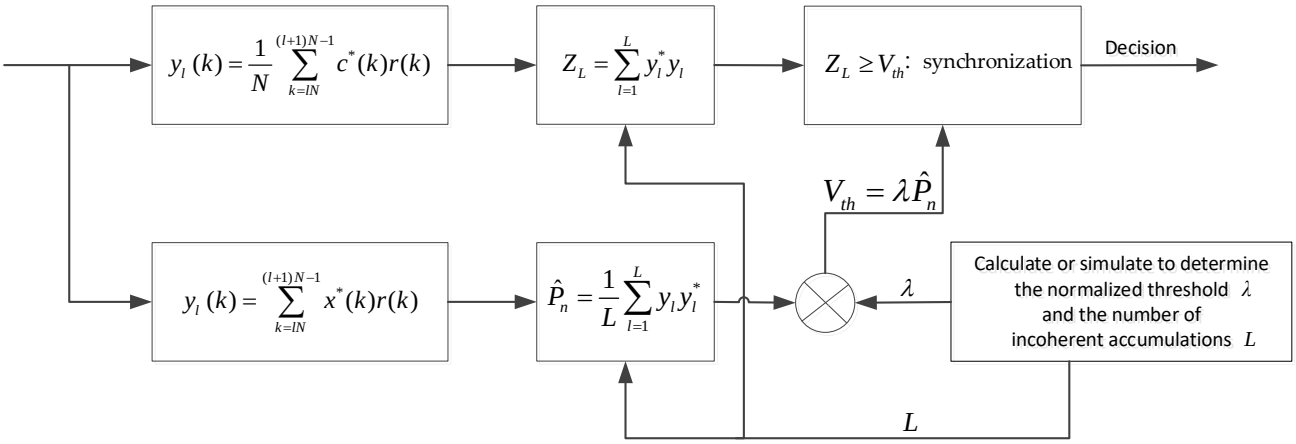


Figure 10. Acquisition algorithm based on adaptive threshold decision.

5.1. Adaptive Threshold Design

The normalization threshold λ and the acquisition threshold V_{th} are defined by (6) and (7) in Section 3. The normalization threshold does not vary with the SNR, while the acquisition threshold is the decision threshold of the test statistic Z. The relationship between λ and V_{th} is $\lambda = V_{th}/P_n$.

The expression of P_{acq} in relation to λ can be obtained from (11), and the relationship between λ and P_{acq} when other variables are fixed is shown in Figure 11. If $P_{acq}(\lambda) > \gamma$, the target requirement is met. Therefore, the minimum and maximum λ are obtained by $P_{acq}(\lambda) = \gamma$. The first solution of the equation is $\lambda_{\min}$, and the second solution is λ_{max}. $\lambda_{\min}$ and λ_{max} are related to the incoherent accumulation length L, the number of decisions M, the symbol signal-to-noise ratio μ and the target acquisition probability γ, that is, $\lambda_{min} = f(L, M, \mu, \gamma)$, $\lambda_{max} = g(L, M, \mu, \gamma)$. We can use γ to constrain the threshold, obtain the maximum and minimum λ by solving the equation, and select a suitable intermediate value as the λ. When the P_{acq} is maximum, λ is λ_{opt}, which is only related to L, M and μ.

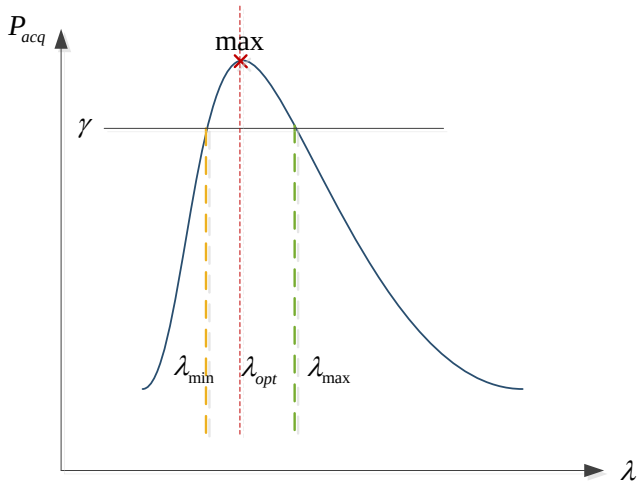


Figure 11. The relationship between λ and P_{acq}.

If we choose λ_{opt} at the maximum P_{acq}, we need to ensure that the selected V_{th} is still within the acceptable range after being affected by the noise estimation error. Because $V_{th} = \lambda P_n$, the impact of noise estimation error $\Delta\hat{P}_n$ on V_{th} at this time (that is, the acquisition threshold estimation error) is $\Delta V = \Delta\hat{P}_n \times \lambda_{opt}$. When the error is within the required range of P_{acq}, its relationship with $V_{\min}$ and $V_{\max}$ is as shown in Figure 12.

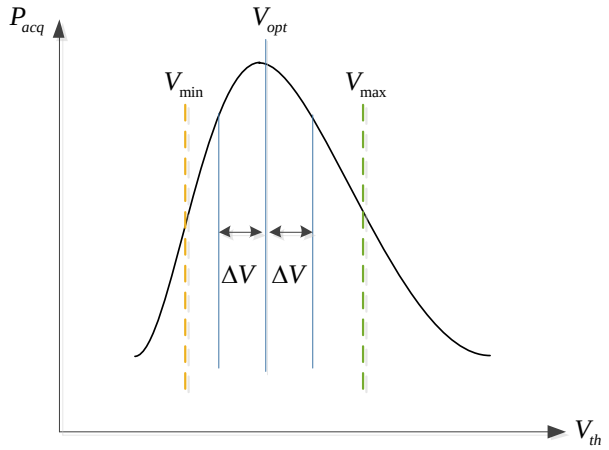


Figure 12. Acquisition threshold estimation error ΔV diagram.

V_{th} is related to L, M, μ and P_n, so we still need to analyze μ and P_n.

5.2. Symbolic SNR μ and Noise Power P_n Estimation

According to Section 5.1, λ is related to μ. The frequency error and code synchronization error will lead to the deterioration of μ, which will affect the selection of V_{th}. Therefore, the influence of frequency error and code synchronization error on SNR is calculated through formula derivation. See Appendix B for the derivation process.

SNR after despreading is

$$SNR = \left[\frac{\sin(\pi fT)}{\pi fT}\right]^2 \frac{NA^2h^2(-\tau T_c)}{\sigma_n^2} = \left[\frac{\sin(\pi fT)}{\pi fT}h(-\tau T_c)\right]^2 \left(\frac{E_s}{N_0}\right) \tag{18}$$

According to (18), μ is affected by the synchronization error of the spread spectrum code and carrier frequency difference. It is assumed that the threshold SNR required by the system is $(E_s/N_0)_{th}$ dB. In the signal acquisition phase, it can be assumed that $|fT| < 1/4$, $|\tau T_c| < 1/4$. Then, through calculation, when $0 < \alpha \leq 1$, SNR deteriorates 1.82 dB $\leq d \leq$ 2.34 dB. The signal-to-noise ratio of the front receiving channel of the

receiver deteriorates to d' and is considered at a maximum of 0.5 dB. Then, the actual working SNR based on logarithmic representation is

$$\mu \geq \left(\frac{E_s}{N_0}\right)_{th} - d - d' \text{ dB} \tag{19}$$

where $\frac{E_s}{N_0} = \frac{E_b}{N_0} + 10\lg m + 10\lg N(\text{dB})$, $m = \begin{cases} 1, & when\ BPSK \\ 2, & when\ QPSK \end{cases}$.

5.3. Noise Estimation Based on Auxiliary Channels

Since $V_{th} = \lambda P_n$, when λ is constant, V_{th} is only related to P_n. The estimator of P_n is $\hat{P}_n$. The real-time estimation of noise variance can be realized based on auxiliary channels. We multiply the received sample sequence with unrelated pseudo-noise sequences (values of ± 1) and add them up in a symbolic period to obtain

$$y_l = \frac{1}{N} \sum_{k=(l-1)N+1}^{lN} x^*(k) r(k) \tag{20}$$

Assuming that the observation length is L_{obs} and the number of auxiliary channels is 1, the estimation result of the noise variance of the auxiliary channel is as follows:

$$\hat{P}_n = M_1 = \frac{1}{L_{obs}} \sum_{l=1}^{L_{obs}} y_l {y_l}^* \tag{21}$$

If based on p auxiliary channels, the estimated noise M_p of p auxiliary channels can be calculated using p uncorrelated pseudo-noise sequence $x(k)$, and its mean is the estimated value of P_n

$$\hat{P}_n = \frac{1}{p} \sum_{i=1}^{p} M_p \tag{22}$$

When the SNR changes at high speed, the number of auxiliary channels can be increased, and the length of observation can be shortened, so the noise estimation can become more accurate.

6. Results and Discussion

The burst spread spectrum based on synchronous overhead has some problems, such as low transmission efficiency, long space exposure time and decline in anti-interception performance. So, the optimal design of the burst spread spectrum is carried out. With P_{acq} better than 0.9999 and SNR of 3 dB before despreading as the design constraint, the design method of burst spread spectrum without synchronization overhead is studied using the BPSK modulation method. According to the relevant background project situation, the data length of 128 symbols can meet the needs of submarine and UAV burst transmission. Therefore, this paper assumes that the design requirements of burst spread spectrum are shown in Table 1:

Table 1. Design requirements.

Design Requirements	Parameters
E_b/N_0	3 dB
data length	16 bytes, 128 symbols
spread spectrum ratio	128
encoding mode	LDPC (1/2)
symbol rate	32 ksps
modulation mode	BPSK
demodulation mode	coherent demodulation
signal duration	4 ms

In addition, $\alpha = 0.3$, and demodulation deterioration is not considered temporarily, while only the carrier frequency difference and code synchronization error are considered, which are both $1/4$, then $d = 1.87$ dB.

6.1. Incoherent Accumulation Length Design

A P_{acq} of at least 0.9999 is required for successful communication. When SNR before despreading is 2, 3, and 5 dB, P_{acq} is simulated according to formula $P_{acq} = (1 - P_f)^{2NL-1} P_d$ (11). The image of P_{acq} changing with λ can be obtained as shown in Figure 13, and the simulation data under various SNRs are given in Table 2.

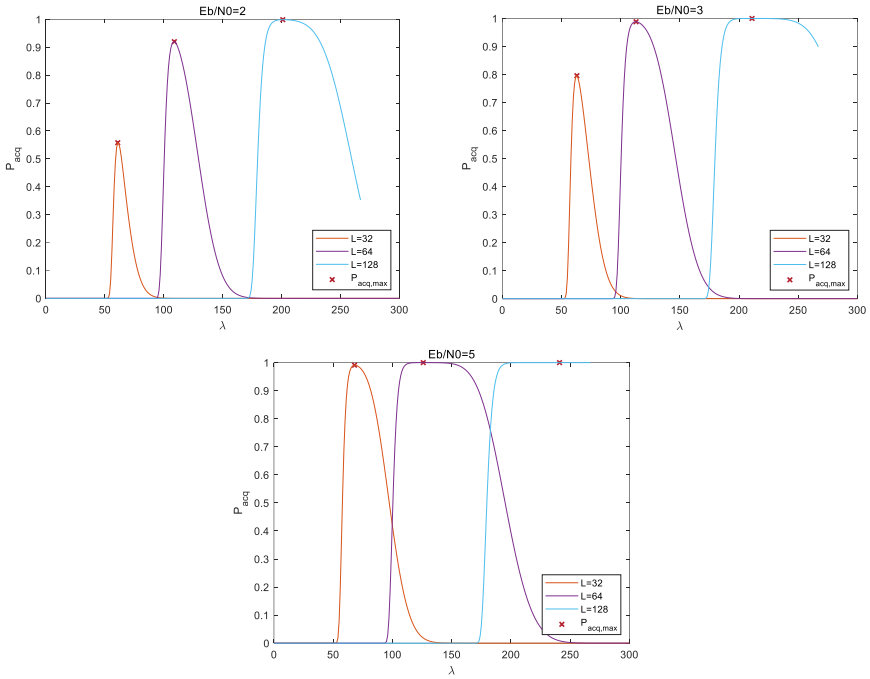


Figure 13. P_{acq} of different L and different SNR varying with λ.

Table 2. Data of the P_{acq} maximum points when SNR before despreading is 2, 3 and 5 dB.

Eb/N0 (dB)	L (Symbols)	λ_{opt}	P_{acq}	P_d	P_f
2	32	61.3	0.5586	0.63	1.4693×10^{-5}
	64	108.7	0.9202	0.9413	1.3865×10^{-6}
	128	201.3	0.9988	0.9992	1.2863×10^{-8}
3	32	62.8	0.796	0.8416	6.7883×10^{-6}
	64	112.7	0.9881	0.9920	2.3684×10^{-7}
	128	**211.4**	**1**	1	2.4605×10^{-10}
5	32	68.2	0.991	0.994	3.6968×10^{-7}
	64	**126.2**	**1**	1	3.5931×10^{-10}
	128	**241.5**	**1**	1	3.8858×10^{-16}

According to the simulation results, the incoherent accumulation length needs to reach 128 symbols under the 3 dB condition. Under the condition of 5 dB, the incoherent accumulation length of 64 symbols can meet $P_{acq} \geq 0.9999$. (Results that meat P_{acq} requirement are shown in bold in the table.) Monte Carlo simulation is carried out for the acquisition with an incoherent accumulation length of 128 at 3 dB. It can be observed in Figure 14 that the Monte Carlo simulation results are basically consistent with the theoretical curve, and the maximum acquisition success probability meets $P_{max} \geq 0.9999$.

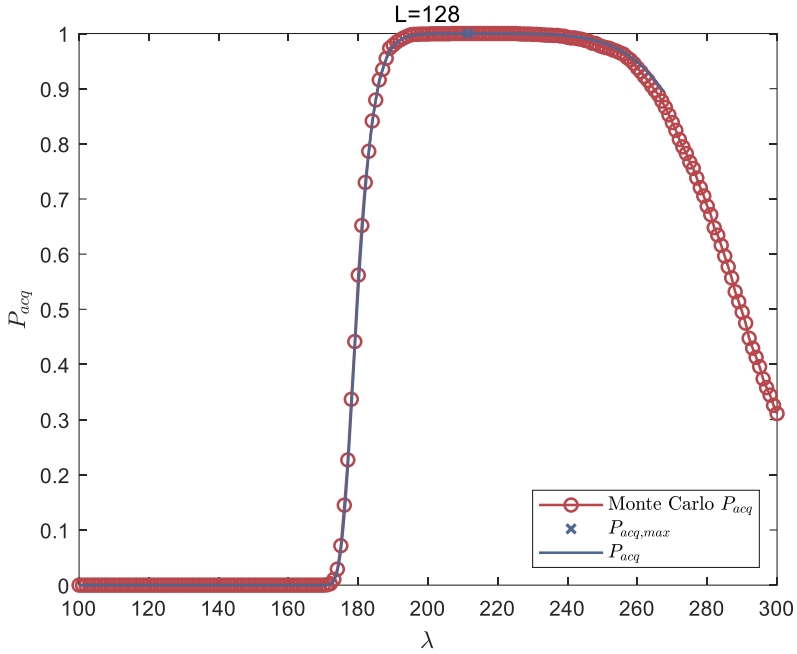


Figure 14. Comparison of theoretical curve and Monte Carlo simulation curve.

However, the adaptive constant false alarm threshold [1,2] did not consider the false alarm caused by a false alarm, and only selected the threshold according to P_f rather than the acquisition success probability. According to this method, the threshold obtained when P_f = 0.0001 is 166. It can be observed from the above figure that the acquisition success probability is close to 0 at this time (the theoretical value is 2.3122×10^{-14}), and the acquisition success probability of the Monde Carlo simulation results is 0. This threshold cannot achieve successful acquisition, and the false alarm value must continue to be reduced. Based on the acquisition success probability, the threshold setting method in this paper is equivalent to giving the exact index basis of false alarm setting on the basis of a constant false alarm threshold, so as to ensure the acquisition success probability of 99.99%.

6.2. Adaptive Threshold Under the Probability of Target Acquisition Success Probability

As can be seen from Table 2, when the SNR before despreading is 3 dB, and L = 128, $P_{acq} \geq 0.9999$. In Figure 15, λ_{min} and λ_{max} are obtained at P_{acq} = 0.9999. In this case, 100,000 Monte Carlo simulations are performed, and the simulation results are shown in Figure 16. Due to the fluctuation of noise variance, the acquisition thresholds also change. Similar to Figure 15, Table 3 can be obtained through simulation.

Table 3. Normalized threshold λ range when Eb/N0 = 3 dB, L = 128.

γ	λ_{opt}	λ_{min}	λ_{max}
0.9999	211.4	205.1	220.9
0.999		199	231.2
0.99		192.6	246.9

According to Section 5.1, because $V_{th} = \lambda P_n$, the acquisition threshold estimation error is $\Delta V = \Delta \hat{P}_n \times \lambda_{opt}$. Taking the median noise P_n = 0.2535 of 100,000 simulations as an example, Table 4 can be calculated based on the data in Table 3. The noise power estimation error requirements $\Delta \hat{P}_n$ under different acquisition success probabilities can be obtained by referring to Tables 4 and 5. For example, if we want $\gamma = 0.9999$, then the noise power estimation errors need to be $0.01 \leq \Delta \hat{P}_n \leq 0.005$. This method can effectively offset the negative effect of noise estimation error on V_{th}.

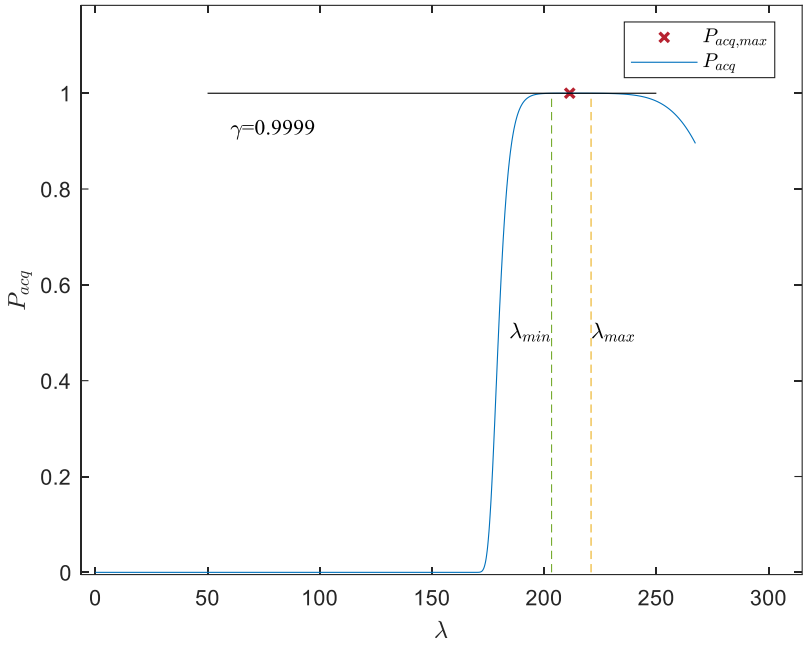


Figure 15. The maximum and minimum normalized thresholds when the target acquisition success probability γ is 0.9999.

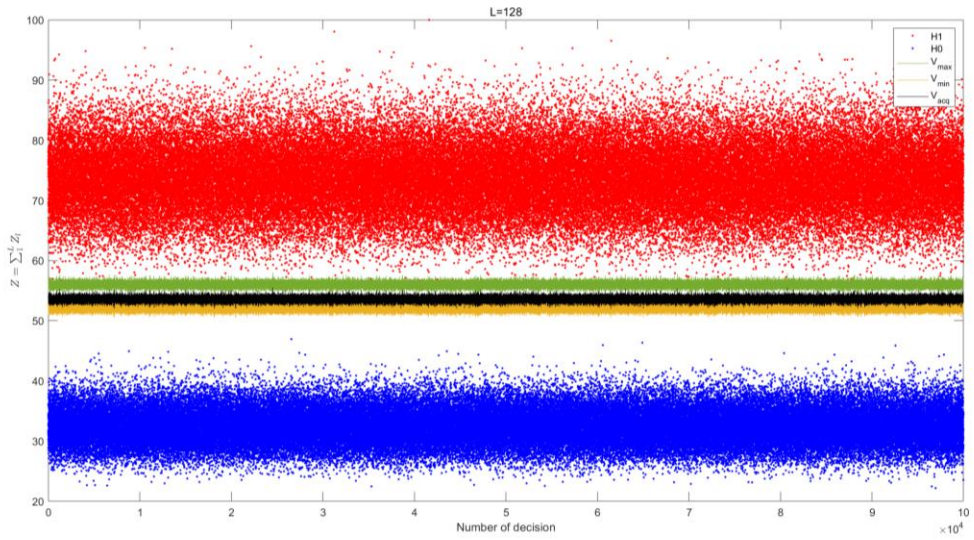


Figure 16. Acquisition simulation diagram when Eb/N0 = 3 dB, L = 128.

Table 4. The acquisition threshold range under different acquisition success probability requirements γ.

P_n	V_{opt}	γ	$V_{\min}$	V_{max}
0.2535	53.5899	0.9999	51.9928	55.9982
		0.999	50.4465	58.6092
		0.99	48.8241	62.5892

Table 5. The estimation acquisition threshold range under different noise estimation errors $\Delta\hat{P}_n$.

$\Delta\hat{P}_n$	ΔV	$V_{opt}-\Delta V$	$V_{opt}+\Delta V$
0.01	2.114	51.4735	55.7015
0.005	1.0570	52.5329	54.6469
0.001	0.2114	53.3785	53.8013

Tables 6 and 7 show the simulation results of noise power under different observation times and numbers of auxiliary channels. Based on the experimental data in Tables 6 and 7, the noise observation error meets the requirement of $P_{acq} \geq 0.9999$. With the increase in observation time and the number of auxiliary channels, the estimated noise error decreases gradually.

Table 6. The estimation of noise power under different observed lengths.

Observed Length L_{obs}	err	bias	RMSE
1	0.0011	2.3631×10^{-4}	0.0333
64	1.6873×10^{-5}	4.8980×10^{-5}	0.0041
128	8.4187×10^{-6}	3.3503×10^{-6}	0.0029

Table 7. The estimation of noise power under different numbers of auxiliary channels.

Numbers of Auxiliary Channels	err	bias	RMSE
1	3.4355×10^{-5}	-3.5409×10^{-5}	0.0059
4	8.7349×10^{-6}	2.2638×10^{-5}	0.0030
8	4.4050×10^{-6}	7.9486×10^{-6}	0.0021

Taking the Monte Carlo simulation of a successful acquisition as an example, as shown in Figure 17, it can be observed that successful acquisition can be achieved when the acquisition threshold V_{th} is between $V_{\min}$ and V_{max}.

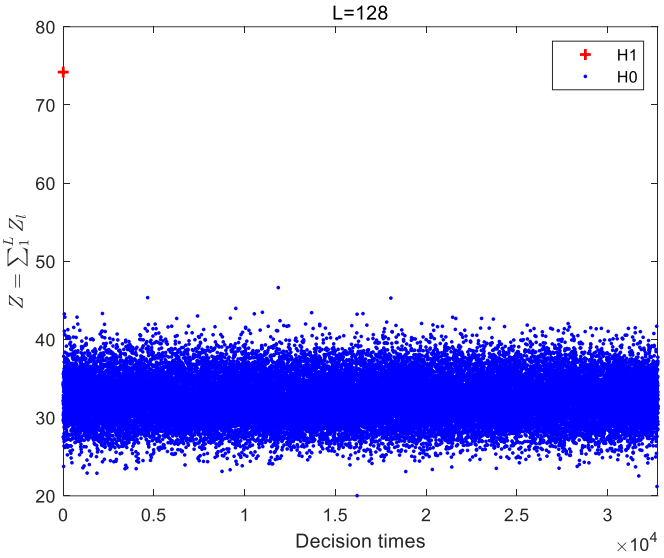


Figure 17. A successful acquisition of the Monte Carlo simulation.

6.3. Hardware Resource Consumption

The hardware of model xc7k325tffg676-2 was selected for simulation on the Vivado 2018 software platform. This paper adopts 8× clock multiplexing with two sample points per chip. As can be seen from the comparison of Tables 8 and 9, LUT decreased by 52.74%, FF decreased by 48.72%, and BRAM decreased by 32.58%.

Table 8. Non multiplexing.

Resource	Utilization	Available	Utilization%
LUT	189,470	203,800	92.97
FF	320,806	407,600	78.71
BRAM	414	445	93.03

Table 9. 8× clock multiplexing.

Resource	Utilization	Available	Utilization%
LUT	81,982	203,800	40.23
FF	125,913	407,600	30.89
BRAM	269	445	60.45

6.4. Frame Transmission Efficiency

Assuming an Eb/N0 of 3 dB, according to the above simulation, in order to achieve a reliable decision, the synchronization overhead of the spread spectrum code synchronization is 128 symbols (after coding) [1,2]. Valid data comprise 128 symbols. Frame length is (synchronization overhead + valid data =) 256 symbols. The data transfer efficiency with synchronization overhead is (valid data length/frame length=) 128/256 = 50%. After the synchronization cost is removed, the data transmission efficiency can be 100%, and the data transmission efficiency can be increased by up to 50%. The total signal length and transmission time are reduced by half, and the concealment of communication is improved.

7. Conclusions

In this paper, a signal structure based on the aperiodic long code spread spectrum is designed to improve the concealment and security of communication based on a transparent forwarding point-to-point satellite communication system. It can achieve reliable signal acquisition without special physical layer synchronization overhead, which can effectively shorten signal transmission time and improve the concealment of communication. The receiver is designed based on a matched filter with high-power clock multiplexing to reduce hardware complexity and hardware resource consumption. In addition, the decision threshold is estimated based on the auxiliary channel in real time to realize the adaptive synchronous decision in the noisy environment and ensure the acquisition success probability. The simulation results show that under typical short burst conditions, the transmission time of a burst signal can be shortened by up to 50% compared with the matching filter acquisition method with synchronization cost, and the acquisition success probability can reach more than 99.99% when Eb/N0 = 3 dB. In this paper, xc7k325tffg676-2 hardware is used to simulate on the Vivado platform, and the hardware resource consumption of the capture matching filter can be reduced by more than 40%.

In future work, we will study the acquisition technology of the burst spread spectrum satellite communication with high dynamic and large frequency offset.

Author Contributions: Conceptualization, S.P. and L.Y.; methodology, S.P. and L.Y.; software, L.Y. and S.P.; validation, L.Y.; formal analysis, S.P. and Y.W.; investigation, L.Y. and Y.T.; resources, S.P. and Y.T.; data curation, Y.T. and Y.W.; writing—original draft preparation, L.Y.; writing—review and editing, S.P., L.Y. and Y.W.; visualization, L.Y.; supervision, S.P. and Y.W.; project administration, Y.T.; funding acquisition, S.P. and Y.T. All authors have read and agreed to the published version of the manuscript.

Funding: This research was funded by an Adaptive Satellite Communication Technology Project, under grant number 2024-173ZD-040.

Data Availability Statement: The original contributions presented in the study are included in the article, and further inquiries can be directed to the corresponding authors.

Conflicts of Interest: Authors Shenfu Pan, Leyu Yin and Yan Wang were employed by the company The 54th Research Institute of China Electronics Technology Group Corporation. The remaining authors declare that the research was conducted in the absence of any commercial or financial relationships that could be construed as a potential conflict of interest.

Abbreviations

The following abbreviations are used in this manuscript:

GEO	Geosynchronous Orbit
MIMO	Multiple-Input Multiple-Output
FFT	Fast Fourier Transform
PMF-FFT	Partial Matched Filter-Fast Fourier Transform
XFAST	Extended replica Folding Acquisition Search Technique
SNR	Signal to Noise Ratio
ISI	Intersymbol Interference

Appendix A. Signal Expression

The spread spectrum signal waveform can be expressed as follows (data symbol d_0 corresponds to spread spectrum code chip $c_0 \sim c_{N-1}$):

$$s(t) = \sum_{p=-\infty}^{\infty} d_p \sum_{m=-\infty}^{\infty} c_m w(mT_c - pT) h_T(t - mT_c) \tag{A1}$$

where d_p is the data symbol sent, the chip period is T_c, the spread spectrum multiple is N and the symbol width is $T = NT_c$. $h_T(t)$ is the signal forming pulse, assumed to be the root rising cosine pulse in this paper, where α is the roll-off factor and has $0 < \alpha \leq 1$ [25]. $w(t)$ is the window function,

$$w(t) = \begin{cases} 1 & 0 \leq t < NT_c \\ 0 & else \end{cases} \tag{A2}$$

The receiver applies a matched filter with an impulse response of $T_c^{-1} h_T(t)$ to the signal in Formula (A1). Then the channel response has the raised cosine characteristic. Considering the complex baseband model in an ideal Gaussian channel, the matched filtered signal can be approximated as

$$r(t) = As(t - \tau T_c) e^{j(2\pi f t + \varphi)} + n(t) \tag{A3}$$

where $s(t - \tau T_c)$ is the baseband signal waveform and $n(t)$ is the noise after matched filtering. In addition, A is the signal amplitude, τ is the normalized signal transmission delay, f is the carrier frequency and φ is the carrier phase after matched filtering.

Sample $s(t - \tau T_c)$ is set according to the chip rate and the sampled data $s(k)$. Assuming that the local spread spectrum code is not strictly aligned with the received signal, the normalized spread spectrum code synchronization error is τT_c. When the signal of Formula (A3) is sampled at $t = kT_c$, the baseband signal after sampling can be expressed as

$$\begin{aligned} r(k) &= As(k) e^{j(2\pi f k T_c + \varphi)} + n(k) \\ &= A \sum_{p=-\infty}^{\infty} d_p \sum_{m=-\infty}^{\infty} c_m w(mT_c - pT) h(kT_c - mT_c - \tau T_c) e^{j(2\pi f k T_c + \varphi)} + n(k) \end{aligned} \tag{A4}$$

Appendix B. Correlation Operation

Using the local spread spectrum code sequence and the received signal after sampling $r(k)$ to perform correlation operations, the despreading data are obtained:

$$\begin{aligned} y_l &= \frac{1}{N} \sum_{k=lN}^{(l+1)N-1} c^*(k) r(k) \\ &= \frac{A}{N} \sum_{k=lN}^{(l+1)N-1} c^*(k) \sum_{p=-\infty}^{\infty} d_p \sum_{m=-\infty}^{\infty} c_m w(mT_c - pT) h(kT_c - mT_c - \tau T_c) e^{j(2\pi f k T_c + \varphi)} \\ &\quad + \frac{1}{N} \sum_{k=lN}^{(l+1)N-1} c^*(k) n(k) \\ &= S_l + \frac{1}{N} \sum_{k=lN}^{(l+1)N-1} c^*(k) n(k) \end{aligned} \tag{A5}$$

where $m = k - q$, q is the delay, since the spread spectrum code is an aperiodic long code, $0 \le q < lN$. S_l in (A5) can be expressed as

$$\begin{aligned} S_l(q) &= \frac{A}{N}\sum_{k=lN}^{(l+1)N-1} c^*(k)\sum_{p=-\infty}^{\infty} d_p \sum_{m=-\infty}^{\infty} c_m w(mT_c - pT)h(kT_c - mT_c - \tau T_c)e^{j(2\pi f k T_c+\varphi)} \\ &= \frac{A}{N}\sum_{k=lN}^{(l+1)N-1} c^*(k)\sum_{p=-\infty}^{\infty} d_p \sum_{q=-\infty}^{\infty} c_{k-q} w(kT_c - qT_c - pT)h(qT_c - \tau T_c)e^{j(2\pi f k T_c+\varphi)} \end{aligned} \tag{A6}$$

When $q = 0$ in (A6), the corresponding signal component is

$$\begin{aligned} S_l(q=0) &= \frac{A}{N}h(-\tau T_c)\sum_{k=lN}^{(l+1)N-1} c^*(k)c(k)\sum_{p=l} d_l \sum_{m=k} w(kT_c - lT)e^{j(2\pi f k T_c+\varphi)} \\ &= \frac{A}{N}h(-\tau T_c)d_l\sum_{k=lN}^{(l+1)N-1} c^*(k)c(k)e^{j(2\pi f k T_c+\varphi)} \\ &\approx \frac{A}{NT_c}h(-\tau T_c)d_l\int_{lNT_c}^{(l+1)NT_c} e^{j(2\pi f t+\varphi)}dt \\ &= Ad_l h(-\tau T_c)\frac{\sin(\pi f T)}{\pi f T}e^{j\varphi_l} \end{aligned} \tag{A7}$$

Its average power is expressed as

$$p_s = E\left[\left(S_{m,q=0}\right)\left(S_{m,q=0}\right)^*\right] \approx A^2h^2(-\tau T_c)\left[\frac{\sin(\pi f T)}{\pi f T}\right]^2 \tag{A8}$$

$q \neq 0$ corresponds to the ISI caused by the channel band limiting effect (time domain trailing effect). If only the ISI of two adjacent symbols is considered, $|q| < N$ can be assumed. p_{J1} is the interference power when q > 0, while p_{J2} is the interference power when $q < 0$. The total interference power can be expressed as

$$p_J = p_{J1} + p_{J2} = \frac{A^2}{N}\left[\sum_{q=1}^{N-1} h^2(qT_c - \tau T_c) + \sum_{q=-N+1}^{-1} h^2(qT_c - \tau T_c)\right] \tag{A9}$$

In summary, the signal after despreading can be approximated as

$$\begin{aligned} Y_l(q) &= \frac{1}{N}\sum_{k=lN}^{(l+1)N-1} c^*(k)r(k-q) \approx Ad_l h(-\tau T_c)\frac{\sin(\pi f T)}{\pi f T}e^{j\varphi_l} + \frac{1}{N}\sum_{k=lN}^{(l+1)N-1} c^*(k)n(k) + n_{2,l}(q) \\ &= Be^{j\varphi_l} + n_{1,l}(q) + n_{2,l}(q) \end{aligned} \tag{A10}$$

where $B = Ah(-\tau T_c)\sin c(fT)$, $n \sim N(0, \sigma_n^2)$, and $n_{1,l} \sim N(0, \sigma_n^2/N)$. $n_{2,l}$ is the noise caused by ISI. The simulation results show that when $N > 32$, $|fT| < 1/4$ and $|\tau T_c| < 1/4$, the interference power of (A8) is at least 20 dB lower than the signal power of (A9), which is negligible in the context of engineering.

References

1. Stojanovic, M.; Freitag, L. Acquisition of direct sequence spread spectrum acoustic communication signals. In Proceedings of the Oceans 2003. Celebrating the Past... Teaming Toward the Future (IEEE Cat. No.03CH37492), San Diego, CA, USA, 22–26 September 2003; Volume 1, pp. 279–286. [CrossRef]
2. Le Nir, V.; Scheers, B. Robust Blind Carrier Frequency Synchronization for Direct Sequence Spread Spectrum Systems. *Electron. Lett.* **2015**, *51*, 425–427. [CrossRef]
3. Zhou, F.; Zhao, L.; Li, L.; Hu, Y.; Jiang, X.; Yu, J.; Liang, G. GNSS Signal Acquisition Algorithm Based on Two-Stage Compression of Code-Frequency Domain. *Appl. Sci.* **2022**, *12*, 6255. [CrossRef]
4. Yang, F.; Wang, G.; Meng, Z.; Guo, X.; Yan, E.; Liu, S. A High Dynamic Weak Spread Spectrum Signal Acquisition Strategy Based on Iterative Local Search. *Electronics* **2022**, *11*, 2881. [CrossRef]
5. Ling, F. Initial Acquisition and Frame Synchronization. In *Synchronization in Digital Communication Systems*; Cambridge University Press: Cambridge, UK, 2017; pp. 67–130.
6. Morelli, M.; D'Amico, A. Maximum Likelihood Timing and Carrier Synchronization in Burst-Mode Satellite Transmissions. *EURASIP J. Wirel. Commun. Netw.* **2007**, *2007*, 065058. [CrossRef]

7. Xing, Y. A New Compatible Fast Acquisition Algorithm for Parameter-varying Spread Spectrum Signals. In Proceedings of the 2018 IEEE 18th International Conference on Communication Technology (ICCT), Chongqing, China, 8–11 October 2018; pp. 1067–1072. [CrossRef]
8. Jiang, B.; Wu, W. A Algorithm of Preamble Acquisition Base on Differential Correlation Module for CDMA System. In Proceedings of the 2018 12th International Symposium on Antennas, Propagation and EM Theory (ISAPE), Hangzhou, China, 3–6 December 2018; pp. 1–4. [CrossRef]
9. Sun, Y.; Jiang, H.; Yi, L.; Hu, W.; Zhuge, Q. Preamble Design for Joint Frame Synchronization, Frequency Offset Estimation and Channel Estimation in Burst Mode Coherent PONs. In Proceedings of the 2024 Optical Fiber Communications Conference and Exhibition (OFC), San Diego, CA, USA, 24–28 March 2024; pp. 1–3.
10. Chen, H.; Qiao, K.; Tong, Y.-P. A Burst Transmission Synchronization Algorithm for Satellite Communication. *Acta Electron. Sin.* **2023**, *51*, 907–913. [CrossRef]
11. Ding, Z.; Hao, T.; Zeng, N.; Hu, L.; Li, L.; Ding, L.; Yang, F. Design of Distributed Synchronization Header for Short Burst Communication with Low Earth Orbit Satellites. In *Digital Multimedia Communications. IFTC 2023. Communications in Computer and Information Science*; Zhai, G., Zhou, J., Ye, L., Yang, H., An, P., Yang, X., Eds.; Springer: Singapore, 2024; Volume 2066.
12. Baeza, V.M.; Ha, V.N.; Querol, J.; Chatzinotas, S. Non-coherent massive MIMO integration in satellite communication. In Proceedings of the 39th International Communications Satellite Systems Conference (ICSSC 2022), Stresa, Italy, 18–21 October 2022; pp. 200–205. [CrossRef]
13. Wu, Y.; Mei, R.; Xu, J. Non pilot data-aided carrier and sampling frequency offsets estimation in fast time-varying channel. *Big Data Res.* **2024**, *36*, 100461. [CrossRef]
14. Lee, D.-U.; Kim, H.; Jones, C.R.; Villasenor, J.D. Pilotless Frame Synchronization via LDPC Code Constraint Feedback. *IEEE Commun. Lett.* **2007**, *11*, 683–685. [CrossRef]
15. Spangenberg, S.M.; Scott, I.; McLaughlin, S.; Povey, G.J.; Cruickshank, D.G.; Grant, P.M. An FFT-based approach for fast acquisition in spread spectrum communication systems. *Wirel. Pers. Commun.* **2000**, *13*, 27–55. [CrossRef]
16. Zhongyuan, B.; Bo, L.; Wen, C. A two-stage fast pseudo-code acquisition algorithm based on pmf-fft. In Proceedings of the 2020 IEEE Asia-Pacific Microwave Conference (APMC), Hong Kong, 8–11 December 2020; IEEE: New York, NY, USA, 2020; pp. 982–984.
17. Qi, J.; Luo, F.; Song, Q. Fast acquisition method of navigation receiver based on folded PMF-FFT. In Proceedings of the 2014 IEEE Computers, Communications and IT Applications Conference, Beijing, China, 20–22 October 2014; IEEE: New York, NY, USA, 2014; pp. 62–66.
18. Liu, J. Status and development of the Beidou navigation satellite system. *J. Telem. Track. Command.* **2013**, *34*, 1–8. [CrossRef]
19. Xu, H. Research on GPS P-Code Direct Acquisition Technology. Master's Thesis, National University of Defense Technology, Changsha, China, 2017.
20. Nie, Y. Using DOP algorithm to evaluate jamming efficiency in GPS jamming tests. *Electron. Inf. Warf. Technol.* **2017**, *5*, 58–62. [CrossRef]
21. Zeng, F.; Ouyang, X.; Xu, H.; Lü, D. Improved Long-code Direct Acquisition Algorithm Based on Time-frequency Fusion. *Dianzi Yu Xinxi Xuebao/J. Electron. Inf. Technol.* **2019**, *41*, 309–316. [CrossRef]
22. Yang, C. FFT Acquisition of periodic, aperiodic, puncture, and overlaid code sequences in GPS. In Proceedings of the GPS Institute of Navigation, Salt Lake City, UT, USA, 11–14 September 2011; pp. 137–148.
23. Zhao, P.; Yao, Y. An ambiguity resolving algorithm for XFAST acquisition with less computational amount in satellite navigation. *Telecommun. Eng.* **2017**, *57*, 1205–1212. [CrossRef]
24. Tang, X.; Yong, S.; Wang, F. Performance of XFAST in the presence of code Doppler. *J. Commun.* **2010**, *31*, 54–59. [CrossRef]
25. Viterbi, A.J. *CDMA Principles of Spread Spectrum Communication*; Addison-Wesley Pub.: Redwood City, CA, USA, 1995.
26. Gil, A.; Segura, J.; Temme, N.M. Algorithm 939: Computation of the Marcum Q-function. *ACM Trans. Math. Softw. (TOMS)* **2014**, *40*, 1–21. [CrossRef]
27. Khan, M.A.; Bicholia, D.; Dubey, R. Comparison of Rayleigh & Ricean Fading Channels using BPSK, QPSK & 16-QAM Modulation Techniques in terms of BER vs. SNR using RRC FIR Filter with DT OFDM Technique. *Int. J. Eng. Res. Technol.* **2015**, *4*, 620–625.
28. Buzzi, S.; Poor, H.V. Channel estimation and multiuser detection in long-code DS/CDMA systems. *IEEE J. Sel. Areas Commun.* **2001**, *19*, 1476–1487. [CrossRef]
29. Weiss, A.J.; Friedlander, B. Channel estimation for DS-CDMA downlink with aperiodic spreading codes. *IEEE Trans. Commun.* **1999**, *47*, 1561–1569. [CrossRef]
30. Iinatti, J.H.J. On the threshold setting principles in code acquisition of DS-SS signals. *IEEE J. Sel. Areas Commun.* **2000**, *18*, 62–72. [CrossRef]
31. Iinatti, J. Comparison of threshold setting rules for the probability of acquisition in a DS spread spectrum receiver. In *1998 International Zurich Seminar on Broadband Communications. Accessing, Transmission, Networking. Proceedings (Cat. No. 98TH8277)*; IEEE: New York, NY, USA, 1998; pp. 23–28.

Disclaimer/Publisher's Note: The statements, opinions and data contained in all publications are solely those of the individual author(s) and contributor(s) and not of MDPI and/or the editor(s). MDPI and/or the editor(s) disclaim responsibility for any injury to people or property resulting from any ideas, methods, instructions or products referred to in the content.